10th International Conference on Composite Science and Technology
ICCST/10
A.L. Araúo, J.R. Correia, C.M. Mota Soares, et al. (Editors)

TOWARDS AEROACOUSTIC-STRUCTURAL OPTIMIZATION OF COMPOSITE WIND TURBINE BLADES

João M. Mascarenhas*, André C. Marta†, Virgínia N. Infante‡

†Center for Aeronautical and Space Science and Technology, IDMEC/LAETA
†Center of Mechanical Design, IDMEC/LAETA

Instituto Superior Técnico, Universidade de Lisboa
Av. Rovisco Pais 1, 1049-001 Lisboa, Portugal

*joao.mascarenhas@tecnico.ulisboa.pt
†andre.marta@tecnico.ulisboa.pt
‡virginia@dem.ist.utl.pt

Keywords: Multi-disciplinary design optimization, Composite materials, Wind turbine, Shape optimization.

Summary: *The extension of an aeroacoustic wind turbine (WT) blade shape optimization to tackle composite structural mechanics is presented. The existing framework is briefly described, following a detailed description of the composite model developed using a finite element model (FEM) formulation. The internal structure of the WT blade is a spar box, for which a finite element code using shell elements is developed capable of handling isotropic, orthotropic and laminated composite materials. The FEM tool developed showed good agreement with comparable results obtained using a commercial software. The structural analysis capability developed is to be later coupled to the aeroacoustic design framework. This effort paves the way for the ultimate goal of optimizing a WT blade, both external shape for aerodynamic and aeroacoustic performance, and internal sizing for structural response, taking int account multiple disciplines, using a multidisciplinary optimization approach.*

1. INTRODUCTION

Power production from wind energy is an emergent topic due to the awareness of the necessity of renewable sources of energy. Although the production of wind energy does not generate pollutants, there is an impact in human health due to noise production of the rotor of wind turbines. In Rodrigues [1] a multi-disciplinary optimization model was developed, where an aeroacoustic model is coupled to an aerodynamic prediction model with the purpose of the maximizing the energy production while simultaneously reducing the noise generation. In this work, a structural finite element model using shell elements, of an internal box-like spar, is to be coupled to the previously developed aeroacoustic optimization framework. The spar is modeled as an internal box-like structure that follows the external geometry of the blade, adding stiffness

thus diminishing the deflection of the blade under load. The material used for the spar can either be isotropic, orthotropic or laminated composite. A parametrization model of the spar was developed and integrated in the framework optimization.

2. THEORETICAL MODELS

2.1 Aerodynamic Model

A wind turbine is a mechanical device that extracts the kinetic energy of the wind in order to convert it to electrical energy. While wind turbines can either have the axis of rotation horizontal or vertical, the focus of this work is only horizontal-axis wind turbines (HAWT).

The present work follows the work developed by Rodrigues [1], that uses the Blade Element Momentum (BEM) theory, with corrections to account the tip- and hub-losses as well as the turbulent wake state. The BEM model follows the assumptions that there is no aerodynamic interaction between blade elements, the forces on the element are dependent on the lift and drag characteristics of the airfoil shape of the blade and the radial velocity component is neglected. Although the spanwise flow is neglected, this component may induce significant modifications to the aerodynamic behaviour, especially near the root. To increase the accuracy of the BEM model, the airfoil data is corrected using the stall delay model from Du and Selig [2] and the drag adjustments from Eggers et al. [3]. In the BEM iterations, the angle of attack calculated can become very large. To make cover to this wider range of values of angle of attack, the aerodynamic data is extrapolated using the procedure developed in Viterna and Janetzke [4].

Knowing the power curve and the probability density function of the wind, based on a Weibull distribution, it is possible to compute the Annual Energy Production (AEP) as

$$AEP = \sum_{i=1}^{N-1} \frac{1}{2} \left(P(V_{i+1}) + P(V_i) \right) \times f(V_i < V_0 < V_{i+1}) \times 8760, \tag{1}$$

where $P(V_i)$ is the power produced by the wind turbine for a wind velocity of V_i, $f(V_i < V_0 < V_{i+1})$ is the probability of the wind to have a velocity V_0 that is between V_i and V_{i+1} and 8760 is the number of hours per year. The Weibull distribution, using 2 parameters, requires the knowledge of a scaling factor A and a form factor k,

$$h_w\left(V_0\right) = \frac{k}{A} \left(\frac{V_0}{A} \right)^{k-1} \exp\left(- \left(\frac{V_0}{A} \right)^{k} \right). \tag{2}$$

2.2 Aeroacoustic Model

In a wind turbine, the sources of noise can be both mechanic and aerodynamic. According to Brooks et al. [5], the aerodynamic noise can be divided in low frequency noise, turbulent inflow noise and airfoil self-noise. The airfoil self-noise can be divided in Laminar Boundary Layer Vortex Shedding noise (LBL-VS), Turbulent Boundary Layer Trailing Edge noise (TBL-TE), Separation-Stall noise, Trailing Edge Bluntness Vortex Shedding noise (TEB-VS) and Tip

Vortex Formation noise (TVF). In Rodrigues [1] it is only considered the turbulent inflow noise and the five mechanisms of the airfoil self-noise, for considering that the aerodynamic noise dominates over the mechanic noise.

Lowson [6] formulated a model for the inflow turbulence noise, where the sound pressure for high frequencies used is

$$L_{p,inf}^{H} = 10\log_{10}\left(\frac{\rho^2 c_0^4 d}{2r_e^2} L I^2 \frac{M^5 \hat{k}^3 \overline{D}}{\left(1+\hat{k}^2\right)^{7/3}}\right) + 78.4\,, \tag{3}$$

where ρ is the density of the air, c_0 is the speed of sound, d is the section span, L is the turbulence length scale, I is the intensity of the turbulence, M is Mach number, $\overline{D}$ is the effect of sound directivity, r_e is the distance from the observer and $\hat{k} = k/k_e$ is the quotient between the wave number $k = 2\pi f/U$, where U is the local inflow velocity, and the wave number range of energy-containing eddies $k_e = 3/4L$. The intensity of the turbulence I is a function of the surface roughness z_0 and height z. For the low frequencies, the model adds a correction factor,

$$L_{p,inflow} = L_{p,inf}^{H} + 10\log_{10}\left(\frac{K_c}{1+K_c}\right), \tag{4}$$

where $L_{p,inflow}$ is the sound pressure level for turbulent inflow noise, $L_{p,inf}^{H}$ is the sound pressure level for high frequencies and K_c is a low frequencies correction factor.

The model presented is based on the flow over a flat plate. To account for the geometry of the airfoil, Moriarty et al. [7] developed a correction factor. The total inflow turbulence noise is calculated by summing this correction factor to the model of Lowson [6],

$$L_{p,airfoil} = \Delta L_p + L_{p,flatplate} + 10\,, \tag{5}$$

where ΔL_p is the correction factor for the airfoil geometry and 10 is a fudge factor to match with NLR data.

The airfoil self-noise is the result of interaction between the blade and the turbulence in the flow due to boundary layer and wake phenomenons. As mentioned earlier this noise source can be divided in five mechanisms. The LBL-VS, TBL-TE and Separation-Stall noise can be predicted by the semi empirical scale laws given by Brooks et al. [5] as

$$L_{p,i} = 10\log_{10}\left(\frac{\delta_i M^{f(i)} L \overline{D}}{r_e^2}\right) + F_i(St) + G_i(Re)\,, \tag{6}$$

where δ_i can be either the boundary layer thickness or displacement thickness, $f(i)$ is a value dependent of the noise mechanism and the terms $F_i(St)$ and $G_i(Re)$ are spectral shape functions that are different for each mechanism but that are always dependent of the Strouhal number St and Reynolds number Re, respectively. The TEB-VS and TVF have a similar formulation, with TEB-VS using spectral shape functions based on the trailing edge solid angle Ψ_{TE} and trailing edge thickness h.

Finally, the prediction method developed in Rodrigues [1] consists in dividing the blade in finite segments, for which a certain airfoil shape and span length are considered. This way, the sound pressure level can be computed at each blade noise element and the total sound pressure level generated by the rotor is the result of a summation of noise from each blade element,

$$L^j_{p,total} = 10\log_{10}\left(\frac{N_B}{N_{az}}\sum_i 10^{\frac{L^j_{p,i}}{10}}\right), \tag{7}$$

where N_B is the number of blades, N_{az} is the number of azimuthal positions where the blade is computed, $L^j_{p,i}$ is the total sound pressure level generated by the i^{th} blade noise element at frequency band j. The Overall Sound Pressure Level (OASPL) is then obtained by the summation of the noise levels at every frequency as

$$OASPL = 10\log_{10}\left(\sum_j 10^{\frac{L^j_{p,total}}{10}}\right). \tag{8}$$

Further details about the aeroacoustic model can be found in Rodrigues [1].

2.3 Structural Model

2.3.1 Plane Elasticity

Every element used is defined in plane stress which is a group of problems in the plane elasticity topic, which studies the small deformations in solid continua. Plane stress problems state that stresses regarding normal local coordinates of the element are zero. The relation between the stress and strain fields is given by the constitutive relation,

$$\sigma = \mathbf{D_m}\varepsilon\,, \tag{9}$$

where the constitutive matrix of the material is

$$\mathbf{D_m} = \begin{bmatrix} \dfrac{E_1}{1-\nu_{12}\nu_{21}} & \dfrac{E_1\nu_{21}}{1-\nu_{12}\nu_{21}} & 0 \\ \dfrac{E_1\nu_{21}}{1-\nu_{12}\nu_{21}} & \dfrac{E_2}{1-\nu_{12}\nu_{21}} & 0 \\ 0 & 0 & G_{12} \end{bmatrix}, \tag{10}$$

where E_1 and E_2 are the Young's modulus in the direction of the fibers and transverse to the direction of the fibers, respectively, G_{12} is the shear modulus and ν_{12} and ν_{21} are the Poisson's ratios.

The formulation of the strain vector for each node is

$$\begin{Bmatrix} \varepsilon_{xx} \\ \varepsilon_{yy} \\ \gamma_{xy} \end{Bmatrix} = \begin{Bmatrix} \dfrac{\partial u}{\partial x} \\ \dfrac{\partial v}{\partial y} \\ \dfrac{\partial u}{\partial y} + \dfrac{\partial v}{\partial x} \end{Bmatrix} = \begin{bmatrix} \dfrac{\partial}{\partial x} & 0 \\ 0 & \dfrac{\partial}{\partial y} \\ \dfrac{\partial}{\partial y} & \dfrac{\partial}{\partial x} \end{bmatrix} \begin{Bmatrix} u \\ v \end{Bmatrix}, \tag{11}$$

where u and v are the displacements in the x and y direction, respectively.

The element used in the present work is Q4, which has four nodes, with two degrees of freedom for each node in the in-plane formulation Zienkiewicz and Taylor [8]. To formulate the problem, the total potential energy of each element is used, defined as $\Pi^e = U^e - W^e$, where Π^e is the total potential energy, U^e is the strain energy and W^e is the work done in the element by external forces. The strain energy U^e is equal to the negative work of the internal forces and is defined as

$$U^e = \frac{1}{2}\int_V \varepsilon_m^T \mathbf{D_m} \varepsilon_m \, dV = \frac{h}{2} d_e^{'T} \int_{d\Omega_e} \mathbf{B_m}^\mathbf{T} \mathbf{D_m} \mathbf{B_m} \, d\Omega_e \, d_e^{'} \,, \tag{12}$$

where ε_m is the membrane strain vector of the element, $\mathbf{B_m}$ is the membrane strain matrix, $d\Omega_e$ is the area dimensions of the element and $d_e^{'}$ is the translational displacement vector of the element, $d_{i_e}^{'} = [u_i \quad v_i]^T$.

From this formulation, it is possible extract the stiffness matrix,

$$\mathbf{K_m^e} = h \int_{d\Omega_e} \mathbf{B_m}^\mathbf{T} \mathbf{D_m} \mathbf{B_m} \, d\Omega_e \,, \tag{13}$$

used in the equilibrium equation,

$$\mathbf{K_m^e} \, d_e^{'} = f_e \,. \tag{14}$$

where $f_e$is the vector of applied nodal forces.

2.3.2 Bending Plates

For the current work, the displacement formulation of *Reissner-Mindlin Plate Theory* is used, which is based on the displacement field,

$$\begin{aligned} u_1(x,y,z,t) &= u(x,y,t) - z\theta_y(x,y,t) \\ u_2(x,y,z,t) &= v(x,y,t) + z\theta_x(x,y,t) \\ u_3(x,y,z,t) &= w(x,y,t) \end{aligned} \,, \tag{15}$$

where (u_1, u_2, u_3) and (u, v, w) are the total displacement of the point and the displacement of a point on the midplane, respectively, in the (x, y, z) coordinate directions. θ_x and θ_y are rotations of the transverse normal about x and y axes. The bending strains obtained are

$$\begin{Bmatrix} \varepsilon_{xx} \\ \varepsilon_{yy} \\ \gamma_{xy} \\ \gamma_{xz} \\ \gamma_{yz} \end{Bmatrix} = \begin{Bmatrix} z\dfrac{\partial \theta_y}{\partial x} \\ -z\dfrac{\partial \theta_x}{\partial y} \\ z(\dfrac{\partial \theta_y}{\partial y} - \dfrac{\partial \theta_x}{\partial x}) \\ \dfrac{\partial w}{\partial x} + \theta_y \\ \dfrac{\partial w}{\partial y} - \theta_x \end{Bmatrix} . \tag{16}$$

Note that ε_{zz}=0 and the transverse shear strains are non-zero.

The bending and shear constitutive matrices are given, respectively, by

$$\mathbf{D_b} = \begin{bmatrix} \dfrac{E_1}{1-\nu_{12}\nu_{21}} & \dfrac{E_1\nu_{21}}{1-\nu_{12}\nu_{21}} & 0 \\ \dfrac{E_1\nu_{21}}{1-\nu_{12}\nu_{21}} & \dfrac{E_2}{1-\nu_{12}\nu_{21}} & 0 \\ 0 & 0 & G_{12} \end{bmatrix} \quad \text{and} \quad \mathbf{D_s} = \begin{bmatrix} G_{13} & 0 \\ 0 & G_{23} \end{bmatrix}. \tag{17}$$

Following the same methodology as in the in-plane formulation, the strain energy for the plate theory is

$$U^e = \frac{1}{2}\int_V \varepsilon_b^T \mathbf{D_b} \varepsilon_b \, dV + \frac{\alpha}{2}\int_V \varepsilon_s^T \mathbf{D_s} \varepsilon_s \, dV, \tag{18}$$

$$U^e = \frac{1}{2}\left(\frac{h^3}{12} d_e^{''T} \int_{d\Omega_e} \mathbf{B_b}^{\mathbf{T}} \mathbf{D_b} \mathbf{B_b} \, d\Omega_e \, d_e^{''} + \alpha h d_e^{''T} \int_{d\Omega_e} \mathbf{B_s}^{\mathbf{T}} \mathbf{D_s} \mathbf{B_s} \, d\Omega_e \, d_e^{''} \right), \tag{19}$$

where α is the shear correction factor and is equal to $5/6$, $\varepsilon_b = [\varepsilon_{xx} \quad \varepsilon_{yy} \quad \gamma_{xy}]^T$ and $\varepsilon_s = [\gamma_{xz} \quad \gamma_{yz}]^T$ are the bending and shear extension vectors, for each node of the element and $\mathbf{B_b}$ and $\mathbf{B_s}$ are the bending and shear strain matrices. The displacement vector for each node is $d_{i_e}^{''} = [w_i \theta_{x_i} \theta_{y_i}]^T$.

The stiffness matrices for bending and for shear contributions are then

$$\mathbf{K_b^e} = \frac{h^3}{12}\int_{d\Omega_e} \mathbf{B_b}^{\mathbf{T}} \mathbf{D_b} \mathbf{B_b} \, d\Omega_e, \quad \mathbf{K_s^e} = h\alpha \int_{d\Omega_e} \mathbf{B_s}^{\mathbf{T}} \mathbf{D_s} \mathbf{B_s} \, d\Omega_e \,, \tag{20}$$

which are used in the equilibrium equation,

$$\left(\mathbf{K_b^e} + \mathbf{K_s^e}\right) d_e^{''} = f_e \,. \tag{21}$$

To avoid computational problems of shear locking, the methodology of reduced integration for the shear contribution of the stiffness matrix is used.

2.3.3 Plane Element in Local Coordinates

The formulation of the shell element couples the effects of membrane and bending in the energy expression (see Zienkiewicz and Taylor [8]). It is important to note that the in-plane forces do not affect the bending deformations and vice-versa and the $\theta_{\hat{z}_i}$ do not enter in the definition of the displacements of either mode.

2.3.4 Drilling Degree of Freedom

The formulation presented so far generates problems with singularities when the nodes defined are *coplanar*, that ia when all elements surrounding the node lay in the same plane. These kind of problems can also occur in *quasi-coplanar* situations. The sixth equilibrium equation for the *coplanar* nodes is

$$\overline{\mathbf{K}}_{\theta_{\mathbf{z_{rs}}}} \overline{\theta}_{z_i} = 0 \,, \tag{22}$$

where $\overline{\theta}_{z_i}$ is the local drilling rotation degree for node i and gives $\overline{\theta}_{z_i} = 0$, avoiding singularities.

For this addition, it is then necessary to define which nodes are *coplanar* and *non-coplanar*. As presented in Oñate [9], this process is possible by generating a vector normal to each element sharing a the node and verify the angle between their normals. The angle can not be inferior to 5^{o} to account for *quasi-coplanar* nodes.

2.4 Composite Model

Following Reddy [10], the *Equivalent Single Layer Theory* is developed by assuming a linear combination of equations of displacement or stress and the thickness coordinate of every layer. This method is used in the present work due to the simplicity, low computational cost and sufficiently accurate description of the global response for thin and moderately thick laminates.

The modifications to the isotropic and orthotropic materials stiffness matrix are

$$\begin{aligned}
\mathbf{K}^{\mathbf{e}}_{\mathbf{m}_{ij}} &= \textstyle\int_{d\Omega_e} \mathbf{B}_{\mathbf{m}i}^{\mathbf{T}} \sum_{k=1}^{N} \left[(z_{k+1} - z_k)\, \mathbf{D}_{\mathbf{m}}{}^{(k)} \right] \mathbf{B}_{\mathbf{m}j}\, d\Omega_e \\
\mathbf{K}^{\mathbf{e}}_{\mathbf{b}_{ij}} &= \textstyle\int_{d\Omega_e} \mathbf{B}_{\mathbf{b}i}^{\mathbf{T}} \sum_{k=1}^{N} \left[\frac{1}{3} \left(z_{k+1}^{3} - z_k^{3} \right) \mathbf{D}_{\mathbf{b}}{}^{(k)} \right] \mathbf{B}_{\mathbf{b}j}\, d\Omega_e \\
\mathbf{K}^{\mathbf{e}}_{\mathbf{s}_{ij}} &= \alpha \textstyle\int_{d\Omega_e} \mathbf{B}_{\mathbf{s}i}^{\mathbf{T}} \sum_{k=1}^{N} \left[(z_{k+1} - z_k)\, \mathbf{D}_{\mathbf{s}}{}^{(k)} \right] \mathbf{B}_{\mathbf{s}j}\, d\Omega_e .
\end{aligned} \tag{23}$$

where the subscripts $\mathbf{m}$, $\mathbf{b}$ and $\mathbf{s}$ refer to membrane, bending and shear, respectiely.

Since the composite elements are composed by layers, the membrane interferes with the bending results and vice-versa, resulting in a new component of the stiffness matrix where this interaction is accounted,

$$\mathbf{K}^{\mathbf{e}}_{\mathbf{mb}_{ij}} = \int_{d\Omega_e} \mathbf{B}_{\mathbf{m}i}^{\mathbf{T}} \mathbf{D}^{(k)}_{\mathbf{mb}} \mathbf{B}_{\mathbf{b}j} + \mathbf{B}_{\mathbf{b}j}^{\mathbf{T}} \mathbf{D}^{(k)}_{\mathbf{mb}} \mathbf{B}_{\mathbf{m}i}\, d\Omega_e, \tag{24}$$

where $\mathbf{D}^{(k)}_{\mathbf{mb}}$ is given by

$$\mathbf{D}^{(k)}_{\mathbf{mb}} = \sum_{k=1}^{N} \frac{1}{2} \left(z_{k+1}^{2} - z_k^{2} \right) \mathbf{D}_{\mathbf{m}}{}^{(k)}. \tag{25}$$

For each of the constitutive matrices $\mathbf{D}^{(k)}_{\mathbf{a}}$, where $\mathbf{a} = \mathbf{m}, \mathbf{b}, \mathbf{s}$, to account for the angle variation of the material of each ply, it is necessary to apply the transformation $\mathbf{D}^{(k)}_{\mathbf{a}} = \mathbf{T}\mathbf{D}^{(k)}_{\mathbf{a}}\mathbf{T}^{\mathbf{T}}$. The transformation matrix $\mathbf{T}$ used for the membrane and bending cases is

$$\mathbf{T} = \begin{bmatrix} \cos^2(\theta) & \sin^2(\theta) & -\sin(2\theta) \\ \sin^2(\theta) & \cos^2(\theta) & \sin(2\theta) \\ \sin(\theta)\cos(\theta) & -\sin(\theta)\cos(\theta) & \cos^2(\theta) - \sin^2(\theta) \end{bmatrix}, \tag{26}$$

while for the shear case the transformation matrix is

$$\mathbf{T} = \begin{bmatrix} \cos(\theta) & \sin(\theta) \\ -\sin(\theta) & \cos(\theta) \end{bmatrix}. \tag{27}$$

3. IMPLEMENTATION

3.1 Verification of Structural Model

To verify the results of the finite element method, the case represented in Figure 1 was developed. The borders are all free except the ones at $z = 0$, which are fixed. The points represent the nodes where the results are verified and are in $(l_1, 0.8l_2, 0.8l_3)$ and $(0.8l_1, l_2, 0.8l_3)$. For this case $l_1 = l_2 = l_3 = 1m$. The results obtained are compared with the commercial program ANSYS®, using the element SHELL63.

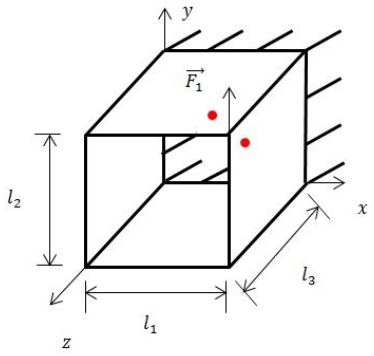

Figure 1. Case of study to verify results using isotropic and orthotropic materials.

The force $\vec{F}_1 = [0 \quad -1000 \quad 0]^T \, N$ is applied on a single node. The case was tested for three different mesh sizes, using grids of 5×5, 10×10 and 20×20 elements for each face, resulting in models with 100, 400 and 1600 elements, respectively.

For the purpose of verifying the results obtained for each degree of freedom, the relative error formulation was used,

$$e_i[\%] = \frac{|Value_{ANSYS_i} - Value_{model_i}|}{|Value_{ANSYS_i}|} \times 100 \tag{28}$$

where e_i is the relative error in percentage, $Value_{ANSYS_i}$ is the value obtained by ANSYS model and $Value_{model_i}$ is the value obtained for the finite element model developed.

For both isotropic and orthotropic cases, it is used a thickness of $0.001m$ and Poisson's ratio of $\nu_{12} = \nu_{21} = 0.25$. For the isotropic material, the Young modulus and shear modulus used are respectively $E_1 = E_2 = 5.4 \times 10^{10} Pa$ and $G_{12} = G_{23} = G_{23} = \frac{E_1}{2+\nu_{12}} Pa$, while for the orthotropic material it is used $E_1 = 5.4 \times 10^{10} Pa$, $E_2 = 1.8 \times 10^{10} Pa$ and $G_{12} = G_{23} = G_{23} = 9 \times 10^9 Pa$, as presented in Lund and Stegmann [11].

3.1.1 Verification of the Model for Isotropic Materials

The results for point $(1, 0.8, 0.8)$ are represented in Figure 2 and for point $(0.8, 1, 0.8)$ are represented in Figure 3.

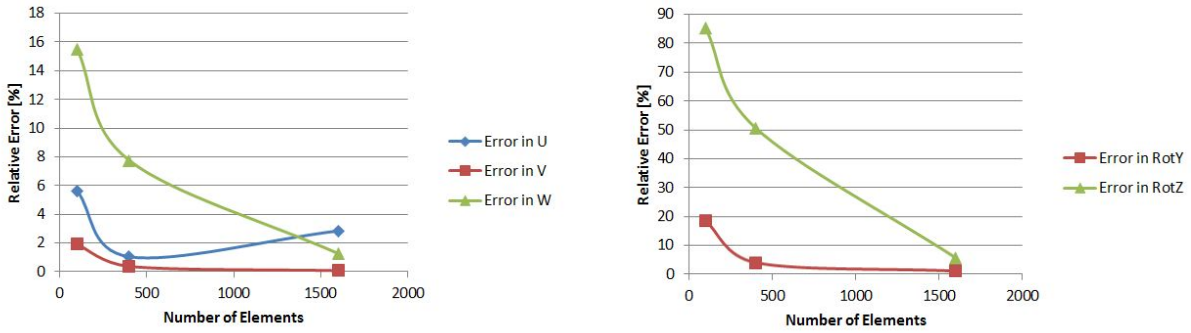

(a) Translational displacements. (b) Rotational displacements.

Figure 2. Errors for the isotropic material at point $(1, 0.8, 0.8)$.

As the number of elements grows, the translational errors for point $(1, 0.8, 0.8)$ tend to values inferior to 5%, although it is visible a small ascendant trend for e_U, while the rotational errors tend to values below 6%. As the number of elements grow, the translational errors for

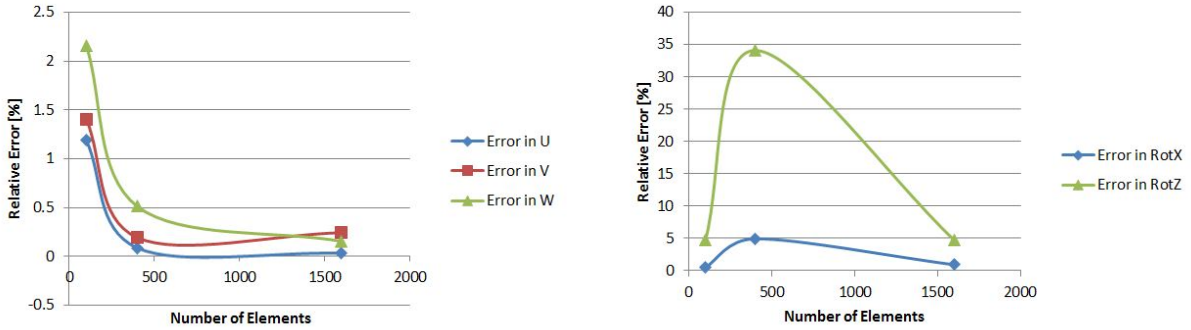

(a) Translational displacements. (b) Rotational displacements.

Figure 3. Errors for the isotropic material at point $(0.8, 1, 0.8)$.

point $(0.8, 1, 0.8)$ tend to values inferior to 0.5% and the rotational errors tend values below 5%. For the finer mesh, corresponding to 10×10 elements divisions of each face, exists instability in the values of the errors, especially for e_{θ_z}.

3.1.2 Verification of the Model for Orthotropic Materials

The representation of the graphical evolution of the errors for point $(1, 0.8, 0.8)$ and point $(0.8, 1, 0.8)$ are in Figure 4 and Figure 5, respectively.

The curves tend to have a similar behavior to the isotropic material results, although errors are a little bit larger. In this case, as the number of elements grows, all relative errors tend to values smaller than 10%.

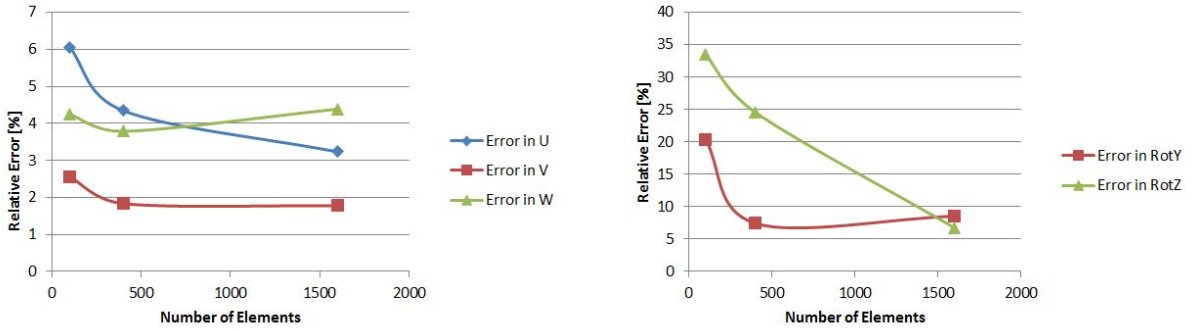

(a) Translational displacements. (b) Rotational displacements.

Figure 4. Error for the orthotropic material at point $(1, 0.8, 0.8)$.

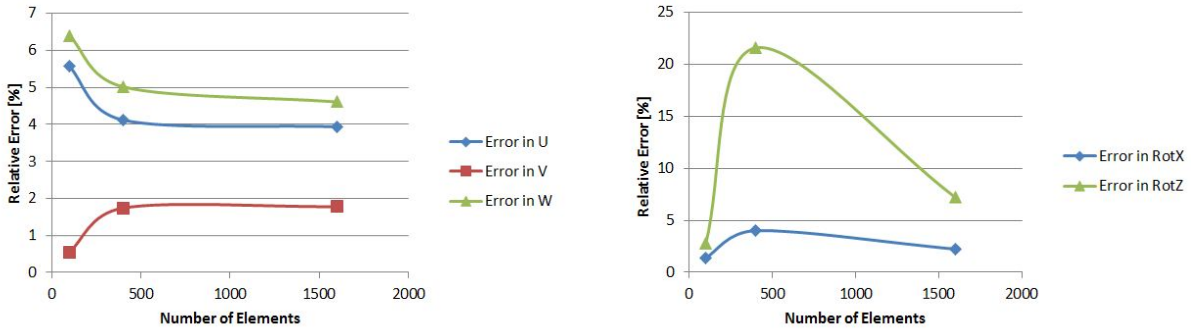

(a) Translational displacements. (b) Rotational displacements.

Figure 5. Error for the orthotropic material at point $(0.8, 1, 0.8)$.

3.2 Verification of the Model for Composite Materials

To verify the composite model, a plane plate model as presented in Figure 6 is used. The reference node is located at $(0.8, 0.8, 0)$, for a plate with dimensions $l_1 = l_2 = 1m$. Two forces are applied, $\vec{F_1} = (0, -1000, 0)\, N$ and $\vec{F_2} = (0, 0, -1000)\, N$. The material used is the orthotropic material previously defined, except when mentioned that two materials are used, corresponding to the orthotropic and the isotropic materials previously defined.

In this case, the ANSYS® element used for the verification is the SHELL181, and a grid of 40×40 elements selected.

In Table 1 it is summarized the relative errors for each displacement variable obtained in the verification for various cases of angles, number of plies, thickness of ply and materials. The orientation of the fibers are relative to the x-axis. Unless otherwise noted, four equal plies are used, totaling a thickness of $0.001m$. When only three plies are used, the middle ply has twice the thickness, thus mantaining the total plate thickness.

As seen in Table 1, the results of the developed composite model show very good agreement with the benchmark values obtained using ANSYS®.

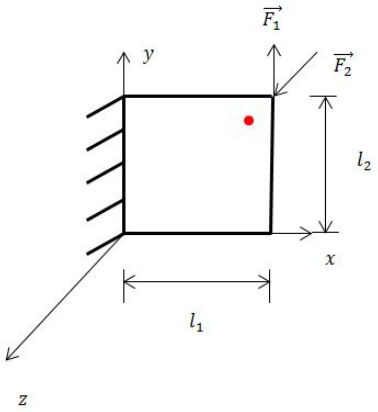

Figure 6. Case of study to verify results of composite model.

Angles	e_U [%]	e_V [%]	e_W [%]	e_{θ_X} [%]	e_{θ_Y} [%]
$0°$	5.148	1.949	3.310	1.564	3.345
$90°$	3.913	2.797	3.660	0.945	3.713
$30°$	2.845	3.288	3.598	4.292	3.641
$60°$	2.323	3.149	2.400	2.618	2.312
$45°$	0.681	3.558	2.737	5.792	2.589
$(15°/-45°/15°)^{\dagger}$	1.336	3.571	3.889	2.562	4.108
$(15°/-45°/15°)^{\dagger *}$	1.176	1.452	3.417	1.894	3.648
$90°/0°/90°/0°$	3.440	1.359	3.430	1.333	3.472
$90°/0°/0°/90°$	2.434	2.316	3.585	1.073	3.626
$60°/30°/-60°/30°$	0.942	7.875	3.153	3.834	3.138
$23°/-5°/-17°/88°$	2.697	3.241	3.344	1.925	3.421

† non-equal thickness between plies * two materials

Table 1. Summary of the values achieved for laminated plate with a grid of 40×40.

4. CONCLUSIONS

In the present work, a finite element model was developed and verified successfully with the commercial program ANSYS, for various geometries, loadings, materials and boundary limits. The model tends to very small values of the relative error, as the number of elements grows. For the composite model, with 1600 elements, the relative error never exceeds 8%.

Current efforts are now focused on merging this development into the wind turbine blade aeroacoustic design framework. Ultimately it will be possible to exercise the multidisciplinary design tool in optimization problems involving functions of interest dealing simultaneously with aerodynamics, acoustics and composite structural mechanics.

ACKNOWLEDGEMENTS

This work was supported by FCT, through IDMEC, under LAETA, project UID/EMS/50022 /2013.

References

[1] S.S. Rodrigues, *Aeroacoustic Optimization of Wind Turbine Blades*. Master Thesis, Instituto Superior Técnico, Universidade de Lisboa, 2012.

[2] Z. Du and M. Selig, *A 3-D stall-delay model for horizontal axis wind turbine performance prediction*. AIAA-98-0021, Proc. 1998 ASME Wind Energy Symposium, Reno, NV, 1998. doi:10.2514/6.1998-21.

[3] A. Eggers, K.Chaney, and R. Digumarthi, *An assessment of approximate modeling of aerodynamic loads on the UAE rotor*. AIAA-2003-868, Proc. 41st Aerospace Sciences Meeting and Exhibit, Reno, NV, 2003. doi:10.2514/6.2003-868.

[4] L. Viterna and D. Janetzke, *Theoretical and experimental power from large horizontal-axis wind turbine*. Report NASA-TM-82944, NASA Lewis Research Center, 1982.

[5] T. Brooks, D. Pope and M. Marcolini, *Airfoil Self-Noise and Prediction*. Report NASA-RP-1218. National Aeronautics and Space Administration, USA, 1989.

[6] M.V. Lowson, *Assessment and Prediction of Wind Turbine Noise*. In Department of Trade and Industry W/13/00284/REP. Department of Trade and Industry, 1993.

[7] P. Moriarty, G. Guidati, and P. Migliore, *Recent improvement of a semi-empirical aeroacoustic prediction code for wind turbines*. AIAA-2004-3041, Proc. 10th AIAA/CEAS Aeroacoustic Conference, Manchester, UK, 2004. doi:10.2514/6.2004-3041.

[8] O. C. Zienkiewicz and R. L. Taylor, *The Finite Element Method - Volume 2: Solid Mechanics*. Butterworth Heinemann, 5th edition, 2000. ISBN:0750650559.

[9] E. Oñate, *Structural Analysis with the Finite Element Method. Linear Statics. vol. 2 Beams, Plates and Shells*. Springer, 1st edition, 2013. ISBN:9781402087424.

[10] J. N. Reddy, *Mechanics of Laminated Composite Plates and Shells - Theory and Analysis*. CRC Press, 2nd edition, 1945. ISBN:9780849315923.

[11] E. Lund and J. Stegmann, *On Structural Optimization of Composite Shell Structures Using a Discrete Constitutive Parametrization*. Wind Energy, 8:109-124, 2005. doi:10.1002/we.132.